

13,01

Morphological features of micro- and nanoporous silver and copper films synthesized by the substitution reaction method

© P.A. Bezrukov¹, A.V. Nashchekin², N.V. Nikonorov¹, A.I. Sidorov^{1,3,¶}

¹ ITMO University,
St. Petersburg, Russia

² Ioffe Institute,
St. Petersburg, Russia

³ St. Petersburg State Electrotechnical University „LETI“,
St. Petersburg, Russia

¶ E-mail: sidorov@oi.ifmo.ru

Received April 10, 2022

Revised April 10, 2022

Accepted April 11, 2022

The results of a study of the structural features of thin silver and copper films synthesized by the chemical substitution reaction are presented. Silver films were obtained by immersing copper substrates in a solution of silver nitrate. Copper films were synthesized by immersing iron and tin-plated iron substrates in a copper sulfate solution. The study of the morphology and composition of the synthesized layers was carried out using a scanning electron microscope. It has been shown that metal nanoporous layers up to 1 μm thick are formed on the substrates as early as 2–3 s after the start of the reaction. The layers consist of microcrystalline hexagonal plates and micro- and nanodendrites. As the reaction time increases, the layers become denser. In this case, the minimum pore size is 20 nm. The synthesized nanoporous films can be used for photocatalytic decomposition of water and enhancement of Raman scattering.

Keywords: morphology, porous film, silver, copper, substitution reaction.

DOI: 10.21883/PSS.2022.08.54634.342

1. Introduction

One promising method of using solar energy is photocatalytic decomposition of water to produce hydrogen fuel. Development of efficient photocathodes opens prospects for practical application of photocatalytic systems to separate hydrogen from water [1–5]. Photocatalytic properties of micro- and nanoporous layers of metals and semiconductors have been studied in a series of experimental works. It has been shown that the efficiency of electron photoemission can reach 50% [3]. Efficiency of photocatalytic decomposition of water is determined not only by the photocathode material, but also by its structure and morphology. In turn, the latter characteristics depend on the synthesis method of the metallic nanoporous layer. The second important application area of micro- and nanoporous metal layers is bio- and chemical sensors based on Raman scattering [5–12]. When surface plasmons propagate in a porous or fractal metal film, „hot spots“ can occur therein. In such regions, amplitude of the electromagnetic wave field is amplified [13], which is accompanied by increase in Raman scattering intensity. This allows sensitivity of the sensors to be significantly increased [5–11].

As a rule, for the above applications, porous layers are synthesized from metals with high conductivity: Ag, Au, Cu. There are many methods for synthesizing metal nanoporous layers: chemical and vacuum deposition, electron beam lithography, laser ablation, etc. [1–12, 14–18]. However,

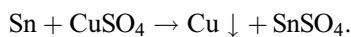
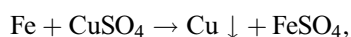
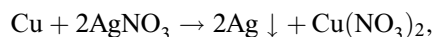
most of these methods are multistep and require complex and expensive equipment. For example, the method for synthesis of gold nanoporous layer using nanosphere lithography described in [16] involves 6 steps. The process for synthesizing a silver nanosphere layer described in [17] includes 5 steps. Moreover, most methods allow creating nanoporous layers in a relatively small area. For example, the method using electron lithography makes it possible to form metallic nanoporous layers only at microscale [14].

The objectives of this paper were to investigate the possibility of synthesizing silver and copper micro- and nanoporous layers by a one-step method using substitution reactions, and to study structure and morphology of the synthesized layers.

2. Materials and methods

Polished plates of copper, electrolytic iron, and iron coated with a tin layer, 5 μm thick, were used as substrates for metal nanoporous layers. Tin layer was deposited by vacuum spraying. The advantage of the metal substrates is that they are a natural conductive base for a photocathode. The substrates had dimensions 10 \times 10 mm². The choice of substrate materials depended on a number of chemical activities of the metals. The following substitution reactions were used to synthesize porous silver and

copper layers



The substrates were washed in acetone prior to synthesis. To synthesize a silver porous layer, copper substrates were immersed in aqueous solution of silver nitrate AgNO_3 (3.75 wt.%). For synthesis of porous copper layers, iron and iron substrates with a tin layer were immersed in aqueous solution of copper sulfate $\text{CuSO}_4 \cdot 5\text{H}_2\text{O}$ (5 wt.%). The reactions were performed at room temperature without stirring the solutions. Reaction duration varied from 2 s to 2 min. Reaction duration and solution concentrations were determined based on preliminary experiments. After the reactions, the samples were washed with distilled water and dried. The structure, composition, and morphology of the porous layers were studied using a JSM 7001 F scanning electron microscope (SEM) (JEOL) equipped with INCA PentaFETx (Oxford Instruments, England) energy dispersive X-ray spectroscopy (EDX) system.

3. Results and discussion

Fig. 1, *a* shows an SEM image of a silver layer fragment on a copper substrate. Reaction duration was 4 s. The figure

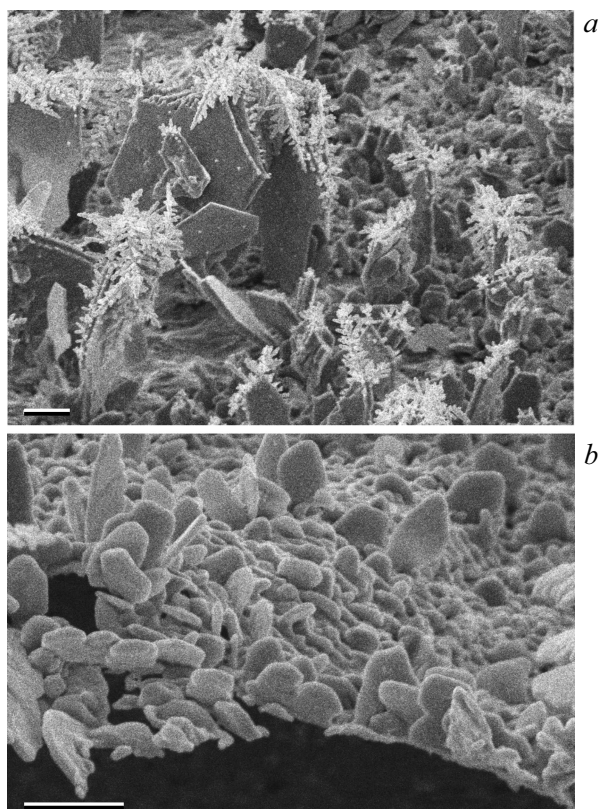


Figure 1. SEM images of silver layers on copper substrate. *a* — reaction duration is 4 s; *b* — initial stage of the reaction. The scales are 1 μm .

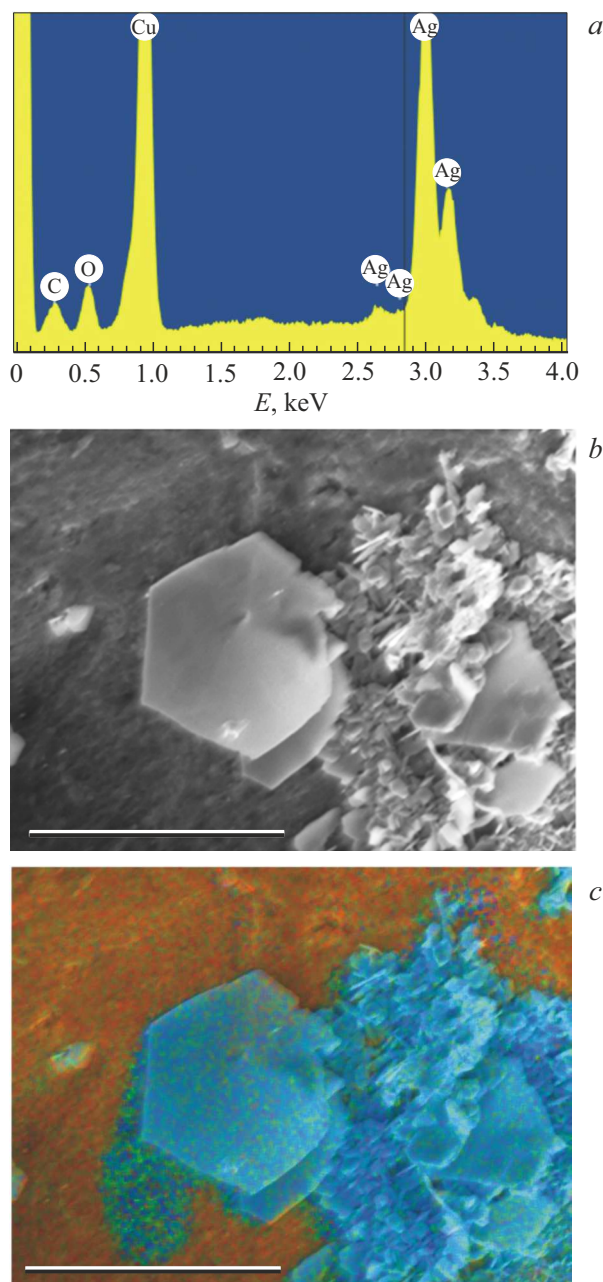


Figure 2. *a* — energy dispersive spectrum of silver layer on a copper substrate. Reaction duration is equal to 4 s; *b* — SEM image of analyzed region; *c* — EDX map of this region. Silver — blue, copper — brown. The scale is 1 μm .

shows that two types of structures are formed: hexagonal silver plates (see also Fig. 2, *b*) and fractal microdendrites. The average thickness of silver plates is 100–200 nm, and the transverse size reaches 3 μm . The shape of the plates is illustrative of their crystalline state. The figure shows that microdendrites grow on the faces of the silver plates, so they appear after plate formation. Length of microdendrites reaches 3 μm . At the initial stage of the reaction, microdendrites are absent, and the layer consists only of plates smaller than 1 μm (Fig. 1, *b*). Some of these

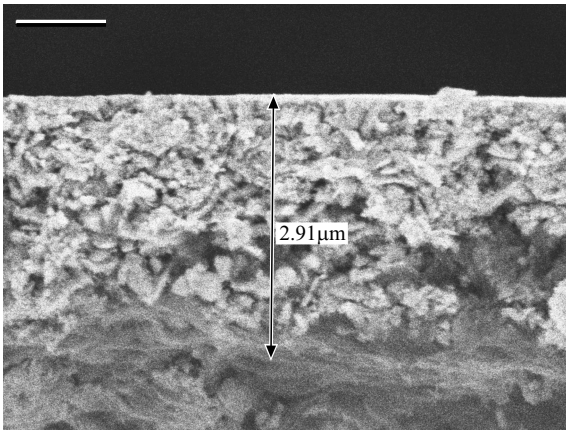


Figure 3. SEM image of cross section of silver layer on a copper substrate. Reaction duration is 2 min. The scale is equal to 1 μm .

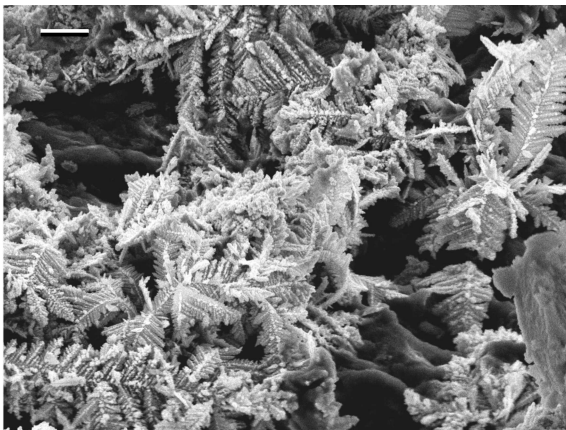


Figure 4. SEM image of copper layer on an iron substrate. Reaction duration is 4 s. The scale is equal to 1 μm .

plates are irregularly shaped. The composition of the formed structures was confirmed by energy dispersive analysis and EXD map (Fig. 2). Oxygen peak on the spectrum can be associated with the presence of silver and copper oxides in the sample.

As reaction duration increases, the porous layer thickens considerably. Fig. 3 shows a cross-section of a porous layer after a reaction with duration of 2 min. Thickness of the layer in this case is 2.91 μm . The minimum pore size is 20 nm, the maximum — 200 nm.

Fig. 4 shows a SEM image of copper layer on an iron substrate. Reaction duration is 4 s. The figure shows that copper microdendrites grow directly on the surface of the iron substrate, unlike the silver layer, without forming lamellar crystals. This may be due to difference in valence states of copper and silver in a solution: copper ions are in divalent state (Cu^{2+}) and silver ions are in univalent state (Ag^+). Copper microdendrites fill the surface of the substrate with high density. As reaction duration increases, porous copper film thickens considerably, as in the case of the silver film.

Fig. 5 shows a SEM image of copper layer on a tin film. Reaction duration is 10 s. As in the previous case, the porous layer consists of microdendrites. However, concentration of microdendrites, in this case, is higher, and their sizes are smaller. The maximum length of microdendrites does not exceed 1.5 μm . The growth rate of copper microdendrites on a tin film is less than that on an iron substrate. A possible reason for this is presence of a thin oxide film on the surface of the tin film.

Let us consider the structure and morphology of a microdendrite using the example of a copper microdendrite. Fig. 6, *a* shows that the microdendrite consists of a „trunk“ up to 3 μm long, with „branches“ that are 300–800 nm long. „Branches“, in their turn, have „needles“. Length of „needles“ reaches 200 nm, and their thickness is 15–20 nm. On these „needles“ there are „needles“ of smaller size: with length of 20–25 nm and thickness of 10–15 nm (Fig. 6, *b*).

One of the characteristics of fractal microdendrites is their fractal size. Let us assess fractal size of a microdendrite shown on Fig. 6. For such microdendrite, fractal size may be introduced for microscale and nanoscale. According to [19], fractal size of cluster D may be determined from equation

$$N = \rho \left(\frac{R}{R_0} \right)^D.$$

Here R — average cluster size, R_0 — average dimensions of monomers that produce a cluster, N — number of monomers in a cluster, ρ — dimensionless parameter ($\rho \sim 1$), which may be interpreted as fractal density. The assessment provides $D = 2.01$ for microscale and $D = 1.6$ for nanoscale.

The reason for formation of two types of metal structures, hexagonal crystals and dendrites is the following. At the initial stage of the reaction, when concentration of metal ions in a solution near the substrate is high, the material is sufficient to form a solid crystal. But in this case the thin layer of solution near the substrate is rapidly depleted of ions. Since reactions are short and take several seconds, metal ions have no time to move due to diffusion from the

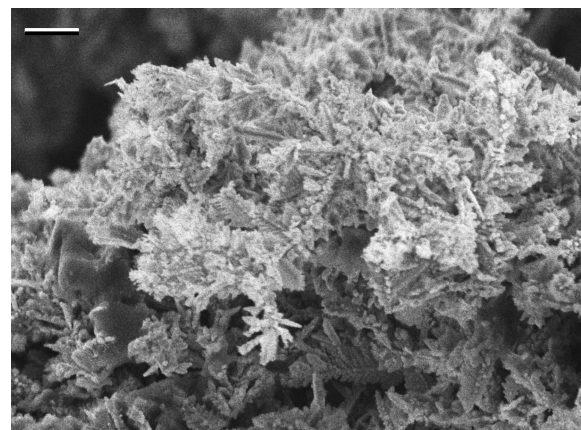


Figure 5. SEM image of copper layer on a tin film. Reaction duration is 10 s. The scale is equal to 1 μm .

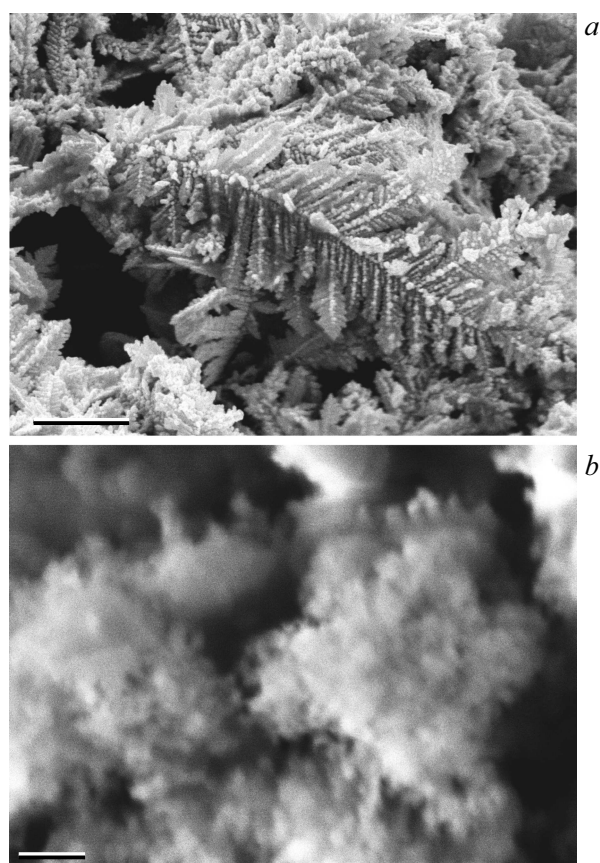


Figure 6. SEM image of copper microdendrite (*a*) and nanodendrites (*b*). Reaction duration is 4 s; *a* — scale is equal to 1 μm ; *b* — scale is equal to 100 nm.

solution volume into the thin reaction layer. This results in change of reaction conditions and crystal formation mechanism. The mechanisms of formation and growth of a fractal ensemble of nanoparticles in a form of a dendrite essentially depend on the method and conditions of its synthesis. As a rule, to describe these processes the aggregation models nanoparticle-cluster [19–23] are used. Most commonly the association use diffusion-limited aggregation and ballistic aggregation as mechanisms. In our case in process of formation and growth of a fractal microdendrite, both mechanisms may participate.

4. Conclusion

Experiments demonstrated that micro- and nanoporous layers of silver and copper may be synthesized using substitution reaction. At the initial stage of silver layer synthesis, silver crystalline plates of hexagonal shape are formed. As the reaction continues, silver microdendrites are formed on them. In case of copper layers, microdendrites arise immediately. As reaction duration increases, nanoporous layers thickens. The advantage of the described method of nanoporous layer synthesis is the fact that it occurs using a single-stage reaction, relatively cheap reagents and does

not require complicated equipment. Another advantage of the method is the possibility to create nanoporous layers on large-size substrates. This approach may be quite attractive for use of nanoporous metal layers in technology of photocatalytic decomposition of water.

Funding

This study was financially supported by the Russian Science Foundation (project No. 20-19-00559).

The electron microscopic studies were performed using the equipment of the Federal Common Use Centre „Materials Science and Diagnostics in Advanced Technologies“, supported by the Ministry of Education and Science of Russia.

Conflict of interest

The authors declare that they have no conflict of interest.

References

- [1] J.K. Stolarczyk, S. Bhattacharyya, L. Polavarapu, J. Feldmann. *ACS Catalysis* **8**, 3602 (2018). DOI: 10.1021/ACSCATAL.8B00791
- [2] Z. Han, F. Qiu, R. Eisenberg, P.L. Holland, T.D. Krauss. *Science* **338**, 1321 (2012). DOI: 10.1126/science.1227775
- [3] Y. Ben-Shahar, F. Scotognella, I. Kriegel, L. Moretti, G. Cerullo, E. Rabani, U. Banin. *Nature Commun.* **7**, 10413 (2016). DOI: 10.1038/ncomms10413
- [4] K. Wu, T. Lian. *Chem. Soc. Rev.* **45**, 3781 (2016). DOI: 10.1039/C5CS00472A
- [5] A. Koya, X. Zhu, N. Ohannesian, A.A. Yanik, A. Alabastri, R. Zaccaria, R. Krahne, W.-C. Shih, D. Garoli. *ACS Nano* **15**, 6038 (2021). DOI: 10.1021/acsnano.0c10945
- [6] X.Y. Lang, L.Y. Chen, P.F. Guan, T. Fujita, M.W. Chen. *Appl. Phys. Lett.* **94**, 213109 (2009). DOI: 10.1063/1.3143628
- [7] Y. Jia, J.D. Ryckman, P.N. Ciesielski, C.A. Escobar, G.K. Jennings, S.M. Weiss. *Nanotechnol.* **22**, 295302 (2011). DOI: 10.1088/0957-4484/22/29/295302
- [8] H. Qiu, Z. Zhang, X. Huang, Y. Qu. *Chem. Phys. Chem.* **12**, 2118 (2011). DOI: 10.1002/cphc.201100205
- [9] C. Ma, M.J. Trujillo, J.P. Camden. *ACS Appl. Mater. Interfaces* **8**, 23978 (2016). DOI: 10.1021/acsmi.6b08191
- [10] R. Jiang, W. Xu, Y. Wang, S. Yu. *New J. Chem.* **42**, 17750 (2018). DOI: 10.1039/C8NJ04060E
- [11] A.S. Pshenova, A.I. Sidorov, T.V. Antropova, A.V. Nashchekin. *Plasmonics* **14**, 125 (2019). DOI: 10.1007/s11468-018-0784-5
- [12] V.V. Strelchuk, O.F. Kolomys, B.O. Golichenko, M.I. Boyko, E.B. Kaganovich, I.M. Krishchenko, S.O. Kravchenko, O.S. Lytvyn, E.G. Manoilo, I.M. Nasieka. *Semicond. Phys. Quant. Electr. Optoelectr.* **18**, 46 (2015). DOI: 10.15407/spqeo18.01.046
- [13] M.I. Stockman. *Electromagnetic theory of SERS*. In: *Surface-enhanced Raman scattering / Eds K. Kneipp, M.Moskovits, H. Kneipp*. Springer, N.Y. (2006). 19 p.
- [14] F.E. Komissarenko, I.S. Mukhin, A.O. Golubok, N.V. Nikonov, M.A. Prosnikov, A.I. Sidorov. *J. MicroNanolithogr. MEMS MOEMS* **15**, 013502 (2016). DOI: 10.1117/1.JMM.15.1.013502

- [15] S. Choi, R.M. Dickson, J. Yu. Chem. Soc. Rev. **41**, 1867 (2012). DOI: 10.1039/C1CS15226B
- [16] M.M.P. Arnob, C. Artur, I. Misbah, S. Mubeen, W.-C. Shih. ACS Appl. Mater. Interfaces **11**, 13499 (2019). DOI: 10.1021/acsami.8b19914
- [17] Z. Shen, D.M. O'Carroll. Adv. Funct. Mater. **25**, 3302 (2015). DOI: 10.1002/adfm.201500456
- [18] R. Ron, E. Haleva, A. Salomon. Adv. Mater. **30**, 1706755 (2018). DOI: 10.1002/adma.201706755
- [19] J. Feder. Fractals. Plenum Press, Springer, Boston (1988). 284 p.
- [20] V.M. Samsonov, Yu.V. Kuznetsova, E.V. Dyakova. ZhTF **86**, 2, 71 (2016). (in Russian).
- [21] B.M. Smirnov. UFN **149**, 2, 177 (1986). (in Russian). DOI: 10.3367/UFNr.0149.198606a.0177
- [22] R. Jullien. Commun. Condens. Mater. Phys. B **13**, 177 (1987).
- [23] T.A. Witten, L.M. Sander. Phys. Rev. B **27**, 5686 (1983). DOI: 10.1103/PhysRevB.27.5686